Polymer Chemistry

Predictive Design of Polymer Molecular Weight Distributions in Anionic Polymerization

Journal:	*Polymer Chemistry*
Manuscript ID	PY-ART-01-2019-000074.R2
Article Type:	Paper
Date Submitted by the Author:	11-Jun-2019
Complete List of Authors:	Domanskyi, Sergii; Clarkson University, Physics Gentekos, Dillon; Cornell University, Department of Chemistry and Chemical Biology Privman, Vladimir; Clarkson University, Physics Fors, Brett; Cornell University, Department of Chemistry and Chemical Biology

Predictive Design of Polymer Molecular Weight Distributions in Anionic Polymerization

Sergii Domanskyi,[a]* Dillon T. Gentekos,[b] Vladimir Privman,[a†] Brett P. Fors[b]*

[a]*Department of Physics, Clarkson University, Potsdam, NY 13676*

[b]*Department of Chemistry and Chemical Biology, Cornell University, Ithaca, NY 14853*

[†]Deceased April 14th, 2018

*To whom correspondence should be addressed. E-mail: domansk6@msu.edu brettfors@cornell.edu

Abstract

Molecular weight distributions (MWD) have a substantial impact on a diverse set of polymer physical and rheological properties, from processability and stiffness to many aspects of block copolymer microphase behavior. The precise MWD compositions of these polymers can be modularly controlled through temporal initiation in anionic polymerizations by metered addition of a discrete initiating species. With the technique described in this work, we identify initiator addition profiles through theoretical modeling which can be used to prepare any desired arbitrary MWD. This kinetic model reproduces experimental MWDs with high fidelity. Our modeling strategy incorporates a detailed kinetic description of polymer initiation and propagation, including the association and dissociation equilibria of the living polymer chain ends. We simplify the kinetic model by incorporating the aggregation phenomena into an effective propagation rate constant k_p, allowing it to vary with the polymer chain length (i). Importantly, this model also yields the ability to predict MWDs at any arbitrary value of monomer conversion during the polymerization. Lastly, we simulate MWDs for a variety of new, yet unmeasured, initiator addition profiles, demonstrating the predictability of this approach.

Introduction

The molecular weight distribution (MWD) of polymers has a profound influence over their physical properties, from processability and bulk macroscale properties to nearly all aspects of block copolymer phase behavior.[1–15] Research in this area has been largely restricted to studying only the effects of dispersity (*Đ*), a parameter which describes the relative span of chains lengths in a given sample. However, morphological and rheological properties of polymers have a significant dependence on the shape and symmetry of their component MWDs. The impact of the MWD shape on such a diverse set of polymer properties clearly demonstrates that modulation of the entire distribution of chain sizes is a promising avenue for fine-tuning the function of polymeric materials without the need to change their chemical structure.[3–8,13] However, until recently this approach has remained largely unexplored due to the lack of general methods that enable the synthesis of polymers with systematically deviating MWDs. In this regard, a general predictive model for targeting any prespecified MWD shape would provide a platform from which scientists and engineers can exploit such phenomena.

Several methods have gained synthetic control of polymer *Đ*.[11,16-24] Although most of these polymerization methods provide excellent control over the relative span of molar masses, they offer only limited control of the absolute shape of polymer MWDs. Our group has recently reported a method for deterministic control of polymer MWD shapes in anionic polymerizations, where the molar quantities of each chain size are dependent on the time at which each chain is initiated.[6–8,25–28] Using this strategy, enabled through the temporal addition of initiator,[7] it has been demonstrated that precise control of the shape and composition of the distribution function profoundly affects polymer physical properties. In further studies of the anionic polymerization of styrene[6] this simple and highly efficient strategy allows the synthesis of functional poly(styrene-*block*-isoprene) copolymers with controlled MWDs, showing that MWD symmetry has a profound influence over the stiffness of these materials.[7] Moreover, in a subsequent study, the thin film domain spacing as well as the bulk morphologies of self-assembled block copolymers could be varied over a wide range simply through modulating the MWD shape of one block.[25] Although this approach is universal and broadly applicable to an array of different monomers and polymerization classes, the resultant MWD derived from any initiator addition rate profile cannot be known *a priori*—a desired MWD must be achieved through a trial and error process. Consequently, in order to fully utilize the shape of polymer MWDs as a handle to control polymer properties, a predictive model

that facilitates access to any arbitrary distribution of chain lengths would offer significant advantages.

To be able to predict MWD composition from a specific initiator addition profile, we began by looking at kinetic models that have been previously developed for anionic polymerization. A simplified model of living and irreversible anionic polymerization kinetics,[29] as well as models developed to simulate MWD in semi-batch living anionic polymerizations were available.[19,30-32] However, we found these systems did not accurately predict the final MWDs in our polymerizations with controlled initiator additions. We hypothesized that the discrepancies in the theoretical and experimental MWDs were because these models did not take into account chain end aggregation, which we believed to be a key kinetic parameter in our system. Theoretical and experimental studies for anionic polymerizations have shown that the rate of polymerization is highly dependent on the degree of polymerization.[33,34] The general consensus for the anionic polymerization of styrene in hydrocarbon solvents is that the growing species exist primarily as dormant associated dimers with a small amount of active dissociated monomeric polystyryllithium species.[35-37] It was proposed that this change in rate was a result of the chain ends existing in equilibrium as inactive associated dimers or active monomers and that this equilibrium would change based on the chain length of the polymer (Scheme 1).[38] Interestingly, others have noted that in radical polymerizations, the termination rate constant is dynamic and dependent on the polymer chain lengths.[39-41] In this study, we develop a model that takes the dynamic aggregation equilibrium into account for the anionic polymerization of styrene and enables the accurate prediction of MWD composition for a wide array of initiator addition profiles. Importantly, we believe this strategy will be applicable to a variety of anionic polymerization methods where chain end aggregation can influence propagation rates.

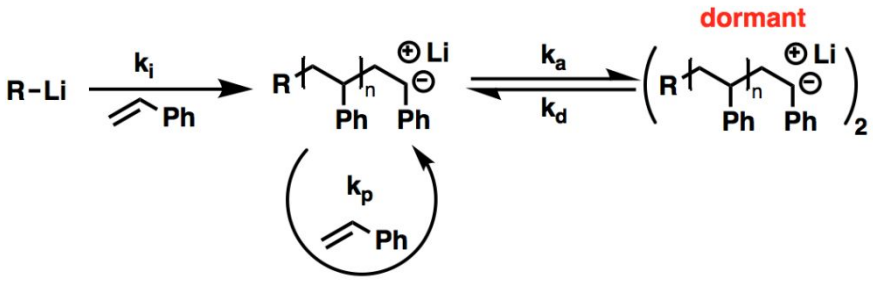

Scheme 1. Initiation, propagation, and aggregation equilibrium in the anionic polymerization of styrene used in this model.

Theoretical Modeling

In this study, we develop a kinetic model of anionic polymerization of styrene which enables the prediction of any arbitrary MWD prepared by adding initiating species, *sec*-butyllithium (*s*BuLi), at predetermined rates and times throughout the polymerization reaction. In order to theoretically model MWDs of arbitrary shape based on the temporal initiation of polymer chains, the kinetics of initiation and propagation need to be understood. Below, we give a description of our approach to this kinetic behavior, describing first the simple kinetic model which neglects the complex phenomena of alkyllithium aggregation and subsequently a more detailed picture that includes aggregation which was required to accurately reproduce the experimental MWDs in this study. Processing of the raw SEC retention time data is described in detail in the Supporting Information (Figure S1 and S2, Equations S1–S4)

In a polymerization mixture of styrene, M, in a hydrocarbon solvent, the typical structure of *s*BuLi is that of a tetrameric aggregate,[38,42,44] $\tilde{I}$, which dissociates into the active initiating species , I.

$$\tilde{I} \underset{k_a}{\overset{k_d}{\rightleftarrows}} 4I \quad (1)$$

Subsequently, active dissociated initiator is rapidly consumed by styrene present in the reaction mixture in the polymer chain initiation step,

$$I + M \overset{k_0}{\rightarrow} N_1 \quad (2)$$

where k_0 is the chain initiation rate constant. The dissociation of aggregated initiator is expected to be slower than that the first monomer addition and initiator association, thus the rate constant k_a, is neglected. Moreover, chain initiation is expected to be much shorter than chain propagation.[34]

$$N_i + M \xrightarrow{k_p} N_{i+1} \quad (3)$$

Equations (2) and (3) constitute a simplified understanding of anionic polymerization which is not sufficient to accurately model our data. This simplified description was studied by Sanchez and coworkers where k_0 and k_p are taken constant, and provided a limited ability to determine the shape of MWDs when the entire quantity of initiator was added at once.[29] Our preliminary study, not detailed here, revealed that no single pair of these two parameters were able to fit at least a subset of our experimental data (several different initiator addition profiles). Therefore, alkyllithium aggregation of living polymer chain ends during chain growth (Scheme 1) has to be accounted for.

The straightforward modeling approach is to assume the rate constant of chain propagation, k_p, that enters Equation (3) uniform for all chain lengths (the innate reactivity of the anionic chain end is constant), while the chains can temporarily form inactive dimers with the rate parameter $\tilde{k}_a(i,j)$,

$$N_i + N_j \underset{\tilde{k}_d}{\overset{\tilde{k}_a(i,j)}{\rightleftarrows}} \tilde{N}_{i,j} \quad (4)$$

where i and j are the degrees of polymerization of the two reacting polymer chains. The associated dimers are dormant and must dissociate before chain propagation can occur, in a process with the dissociation rate constant $\tilde{k}_d$.The dependence of $\tilde{k}_a$ on i and j is non-trivial and unknown, however, shorter chains presumably have a higher probability of creating dormant dimers due to their higher mobility and more accessible active anionic chain ends from the lack of steric bulk; similar to the decreased chain mobility leading to the Trommsdorff-Norrish effect.[45] The short chains can also form dimers with longer chains, and each combination of chain lengths has its own distinct equilibrium constant. Consequently, long chains are expected to dimerize at a much lower rate than shorter chains and thus remain active for longer periods of time than short polymers. Strictly speaking, the *observed* propagation rate constant appears to be dynamic, but this is likely due to the complex aggregation behavior being dependent on the entire statistical distribution of chain lengths, $\{N_{j\geq 1}(t)\}$, which also varies with time and renders the system dynamics challenging to

solve. By absorbing the process of association and dissociation of the polystyryllithium dimers into an average effective rate constant of chain propagation, a function of the chain length, *i*,

$$k_p = \kappa \cdot k_p(i) \quad (5)$$

we avoid solving a complex matrix of equations related to $\tilde{N}_{i,j}$, mentioned above, setting $\tilde{k}_a(i,j) = 0$. In addition, we reserve a monomer-concentration-dependent parameter, κ, to account for a potential dependence on the concentration. Incorporation of such an average rate constant into the reactions in Equations (1)-(3) makes modeling feasible and is approximated by the standard differential rate equations:

(6)

$$\frac{d\tilde{I}}{dt} = -k_d\tilde{I}$$

$$\frac{dI}{dt} = 4k_d\tilde{I} - k_0IM$$

$$\frac{dM}{dt} = -k_0IM - \sum_{i=1}^{\infty} k_p(i)N_iM$$

$$\frac{dN_{i\geq 1}}{dt} = \delta_{1i}k_0IM + (1-\delta_{1i})k_p(i-1)N_{i-1}M - k_p(i)N_iM$$

where δ_{1i} is the Kronecker delta symbol, 0 when $i \neq 1$ and 1 when $i = 1$.

It is important to note that the system description that includes Equation (4), i.e. constant propagation rate and complex dimers aggregation behavior, is not equivalent to an effective rate approach summarized in Equation (6). This question requires a search for functions $\tilde{k}_a$ and $\tilde{k}_d$ which themselves may depend on multiple parameters. Nonetheless, the following sections show that the effective rate approach is suitable for describing our system for a variety of experimental conditions.

Initiator Addition Rates

In order to test the accuracy of the above kinetic model in predicting MWD shapes, we explore a variety of initiator addition profiles shown below. The alkyllithium initiating species was added at various rates and times to the reaction mixture to start the polymerization process. The

total amount of the initiator and monomer in each experiment was kept the same, I_0 and M_0, respectively, such that the final M_n values of the polymers remained constant. We carried out our studies by employing initiator addition profiles from earlier work,[6,7] and also designing two types of complementary profiles. Figure 1 contains initiator addition rates as a function of time. Data from the experiments corresponding to Figure 1B–F are used for demonstration of the predictive power of the model (see Results and Discussion).

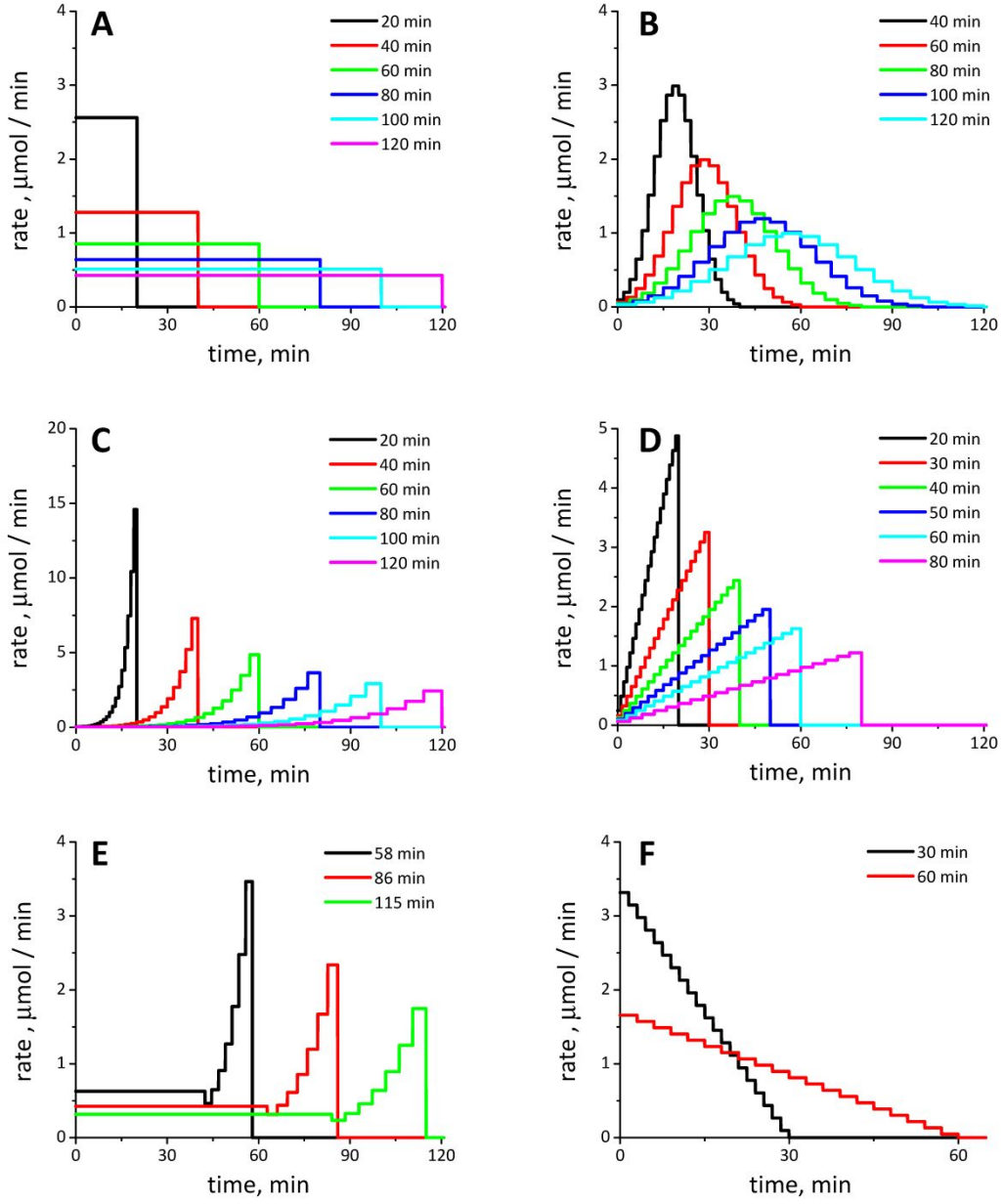

Figure 1. Initiator addition rates following four shapes: (A) constant rate, (B) bell-shaped rate, (C) exponentially increasing rate, and (D) linearly increasing rate, (E) partly constant and then exponentially increasing rate (Tables S1 – S3), and (F) linearly decreasing rate (Tables S4 – S5).

Results and Discussion

Data Fitting and Theoretical Model Parameter Investigation

In the preceding section, we outlined a modeling approach that can be applied to the grand challenge of predicting MWDs for any arbitrary initiator addition profile. Here we show how to utilize it and fit the experimental data. The overall process starts with the development of the theoretical model on a training data set, in this case, the constant rates of initiator addition (Figure 1A). Then, all of the rate parameters in Equation (6) were calculated and optimized. This model was then used to fit the MWDs of all other initiator addition profiles not within the training set, i.e. Figure 1B–F. Initially, as we mentioned previously, the process of the initiator association is neglected, $k_a = 0$, due to fast initiation of the dissociated species. The rate for the initiation process cannot be precisely determined from the considered experimental data due to large differences in the timescales of chain initiation and propagation. Setting the rate k_d to be an order of magnitude larger than the propagation rate for the chains after one monomer addition is sufficient to describe the data. In this work, we set $k_d = 7\ \mathrm{min}^{-1}$ and $k_0 = 8.06\ \mathrm{M}^{-1}\mathrm{min}^{-1}$, determined by optimization during the fitting procedure. The parameter κ is dependent on the initial monomer concentration, M_0, and set to unity except for the dilution experiments in Figure 9. To solve Equation (6), we utilize a standard Runge-Kutta-Fehlberg method (RKF45),[46,47] an algorithm for the numerical solution of differential equations. The resulting MWDs are compared to the preprocessed, experimental data. The nonlinear least squares method is used to find the unknown parameters (rate constants).

The last rate parameter we determined was k_p. We hypothesized that larger polymer chains, having decreased mobility and increased steric bulk, would result in a lower affinity for aggregation to the dormant species and thus have a higher rate of propagation. Therefore, for each experiment with the constant initiator addition rate, the training set described above, we simulated the polymerization process with an unknown dependence of $k_p(i)$ on i, Equation (5), which was initially chosen as a first order polynomial, $k_p(i) = a \cdot i + b$, where a and b are unknown parameters. A simple linear dependence was found insufficient to fit parameters a and b

simultaneously for the entire training set. For this reason, we chose to further explore the relationship between $k_p(i)$ and i. The function found to best fit these data is shown in Figure 2, which illustrates a nonlinear dependence of $k_p(i)$ on i (Equation S5). Importantly, this rate of propagation is in good qualitative agreement with previous studies, which found that the apparent propagation rate constant increases with increasing chain length.[34] This complex scaling behavior may be a result of the complex and dynamic aggregation phenomena when a large number of different molar masses are present.

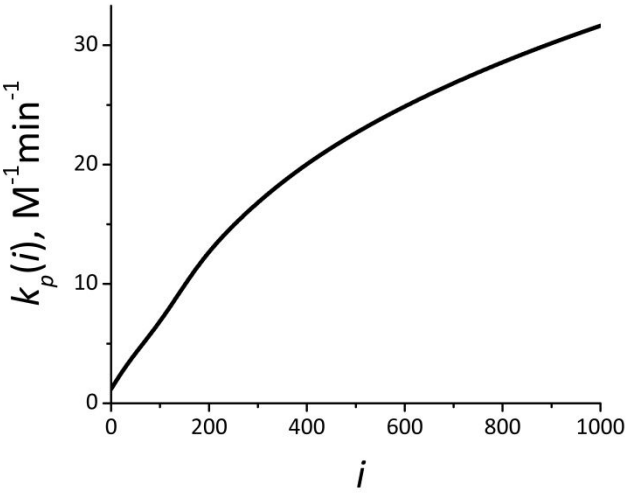

Figure 2. Numerically determined *effective* rate constant as a function of chain length, Equation (S5), that fits the experimental MWDs for the constant rates of initiator addition, Figure 1A.

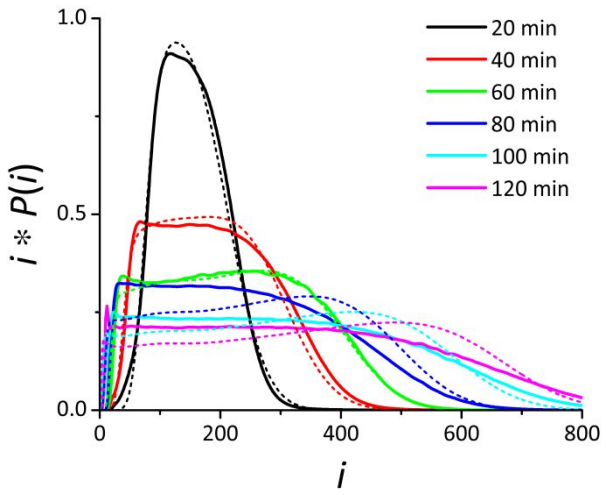

Figure 3. Experimental data (solid lines) and calculated curves (dashed lines) for the constant rate, Figure 1A, used as a training set to determine the average *effective* propagation rate, shown in Figure 2.

Model Validation

Without any modification, the effective propagation rate (Figure 2) was found to accurately describe the MWDs derived from the other rate profiles not within the training data set used to develop the theoretical model (Figure 1B, 1C, and 1D), with the bell-shaped, exponentially increasing, and linearly increasing initiator addition rates. The modeling curves along the experimental data are shown in Figure 4. This model provides a good fit of the experimental MWDs, closely following the shape of each type of initiation profile. Moreover, it is important to note that as the initiation time increases, so does the deviation between experimentally determined MWDs (Figure 4, solid lines) and those that were determined through theoretical modeling (Figure 4, dotted lines). Interestingly, the fits are about equally accurate for each type of initiator addition profile, from constant and linearly increasing rates of addition to more complex profiles such as exponentially increasing and bell-shaped rates. This observation exemplifies the robustness and modularity of this theoretical approach.

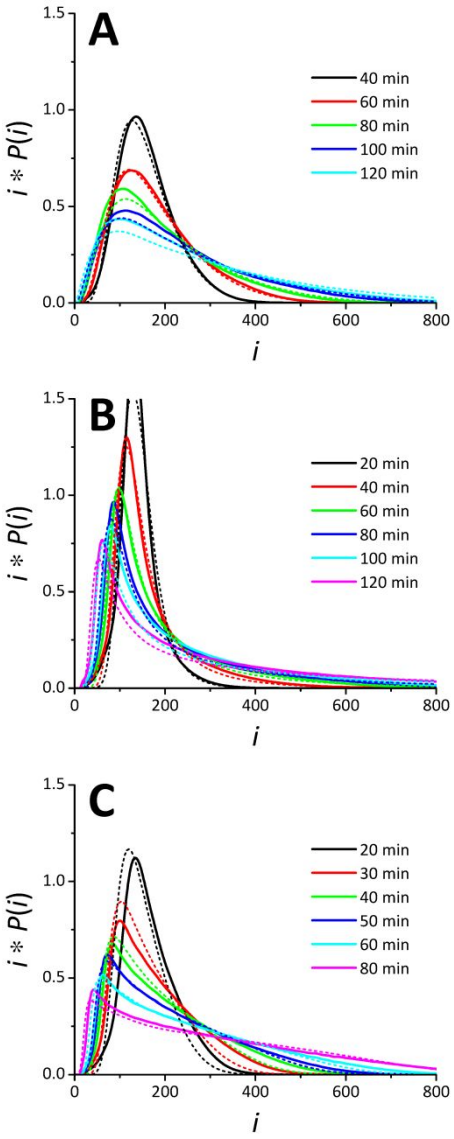

Figure 4. Experimental data (solid lines) and calculated curves (dashed lines) for the average *effective* rate, kept the same for all curves in this plot: (A) bell-shaped rate, (B) exponentially increasing rate, and (C) linearly increasing rate.

One case, where all the initiator was added at once at the beginning of the polymerization reaction, was suboptimal if simulated with the effective rate profile in Figure 2, (Figure 5). However, in this experiment, the initiator is added instantaneously, resulting in a much larger concentration of initiator at the beginning of the reaction and therefore giving different kinetics. This is in contrast to the experiments in which the initiator was added continuously into the system

on the order of an hour or longer. As noted by Sanchez, the concentration of initiator has been shown to dramatically influence the polymerization kinetics as the MWDs are highly dependent on initial conditions.[29,39,40] The small amount of error shown in Figure 5 likely arises from these differences, and a more detailed analysis may require incorporation of the aggregation behavior of the alkyllithium initiator from Equation (1) into the model. However, the fit from the current model is quite reasonable and a more complex discussion of the dynamics in such systems is beyond the scope of the present work.

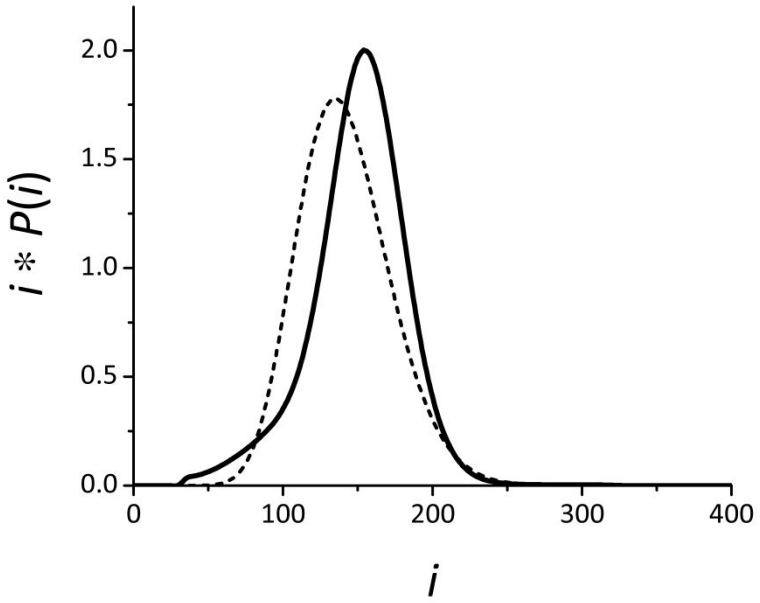

Figure 5. 0-min initiator addition time experimental data (solid line) and a calculated curve (dashed line) for the average *effective* rate shown in Figure 2.

Additional Modeling Considerations

In addition to varying the initiator addition rates and holding the initial monomer concentration constant, M_0, we examined our experimental system with a set of four polymerization experiments with "60 min" constant rate, Figure 1A, using different amounts of solvent resulting in a series of monomer dilutions, α:

$$\alpha = {M_0}/{M_0^*}, \qquad (7)$$

where M_0^* is the new initial concentration of the monomer in the system. For each of the dilution datasets we performed least-square fit of the parameter κ, from Equation (5), while maintaining the propagation rate the same as in Figure 4 ($k_p(i)$ from Figure 2). The fitting of κ is illustrated in Figure 6, where the experimentally measured data curves are shown as solid lines and model fit as dashed lines. The inset of this figure suggests a strong correlation ($R^2 = 0.98$) between the fitted values of κ. The linear fit reveals that:

$$\kappa(\alpha) = -0.27\log_2 \alpha + 0.91. \quad (8)$$

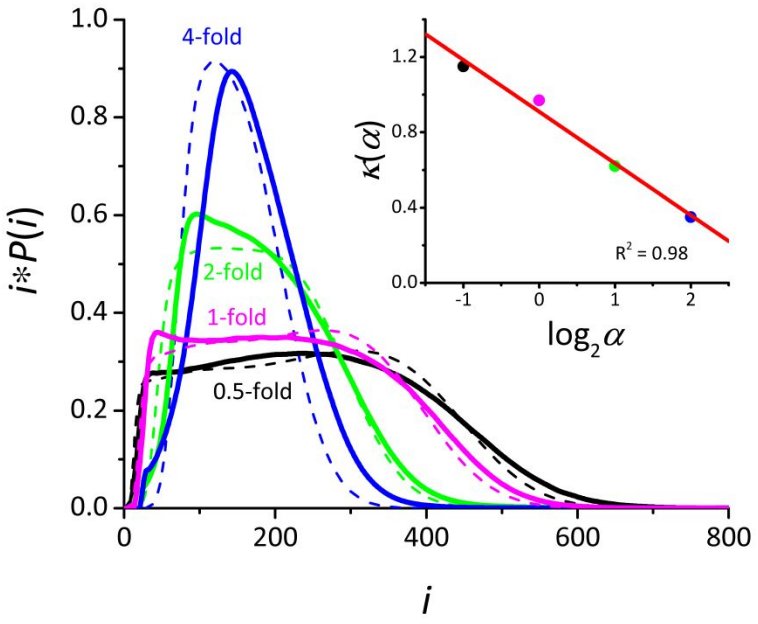

Figure 6. Experimental data (solid lines) and calculated curves, optimizing $\kappa(\alpha)$, (dashed lines) for the constant rate "60 min", Figure 1A (green line), used as a training set to determine dependence of the average *effective* propagation rate, shown in Figure 2, on the system dilution, α. The inset shows individual curves fits (solid dots) for 0.5, 1, 2 and 4-fold dilutions (left to right) color-coded to the distributions in this figure. The line in the inset is the linear fit of these four points.

These concentration experiments show clearly that dilution has a substantial influence on the polymerization reaction kinetics. Additionally, these results elucidate that the κ parameter

decreases nonlinearly with increasing dilution, likely due to the complex dynamics of mixed alkyllithium aggregation.

We have also tested the sensitivity of our model predictions to the input parameters. As expected, the main controlling parameter, k_p, provides good linear control over the MWD shape. The small changes in MWD observed as k_0 and k_d are altered shows that these parameters are in the regime not limiting the system's dynamics. The calculations are shown in Figure 7, exemplified on the 60 min constant initiator addition rate, with $\kappa = 1$. The dotted line is experimental data, the black solid line is calculated with $1.0 * k_p$, $1.0 * k_0$ and $1.0 * k_d$. The blue lines show how the model's response is altered by varying the propagation rate from $0.9 * k_p - 1.1 * k_p$ (blue shaded area). The red and green shaded regions are for the parameters k_0 and k_d, respectively. These two parameters are already large enough not to limit the polymerization dynamics. Even significant decreases in these parameters (here taken as 20-fold) show little change in the overall fit.

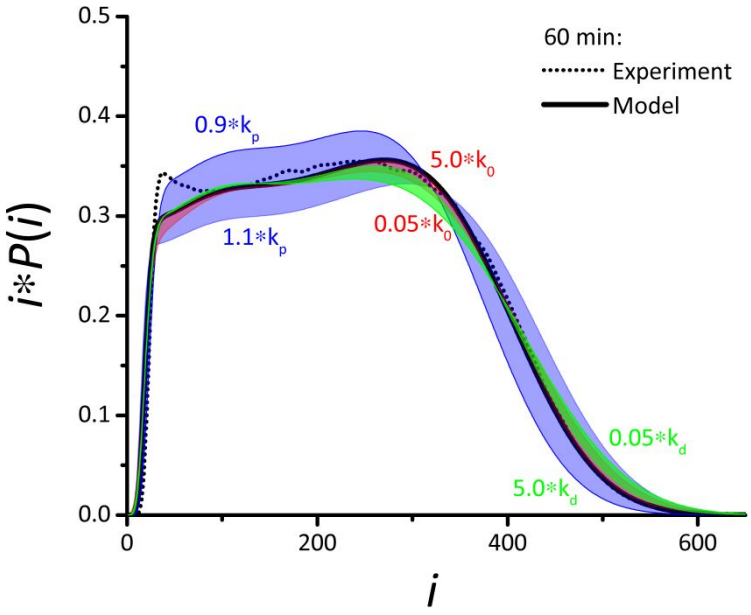

Figure 7. Sensitivity to the model parameters demonstrated by varying the propagation rate, initiation rate and dissociation rates from their optimized values, k_p, k_0 and k_d, respectively.

Theoretical modeling of the type presented in this work is beneficial for providing insight into the dynamics of the polymerization processes. To exemplify this we calculate the MWDs at the times when the monomer conversion is incomplete, see Figure 8, where we model the polymerization process with exponentially increasing rate of initiator addition within 80 min. The five traces shown in Figure 8A demonstrate the polymerization dynamics with the distributions shifting to the higher molecular weights as the chains grow. Figure 8B and 8C show how much monomer remains in the system and the number of polymer chains that have been initiated, respectively. The solid dots on panels (B) and (C) of Figure 8 are color-coded to the times of snapshots in panel (A). This type of analysis at different time points provides insight into the evolution of MWDs over time as more initiator is added to the polymerization reaction.

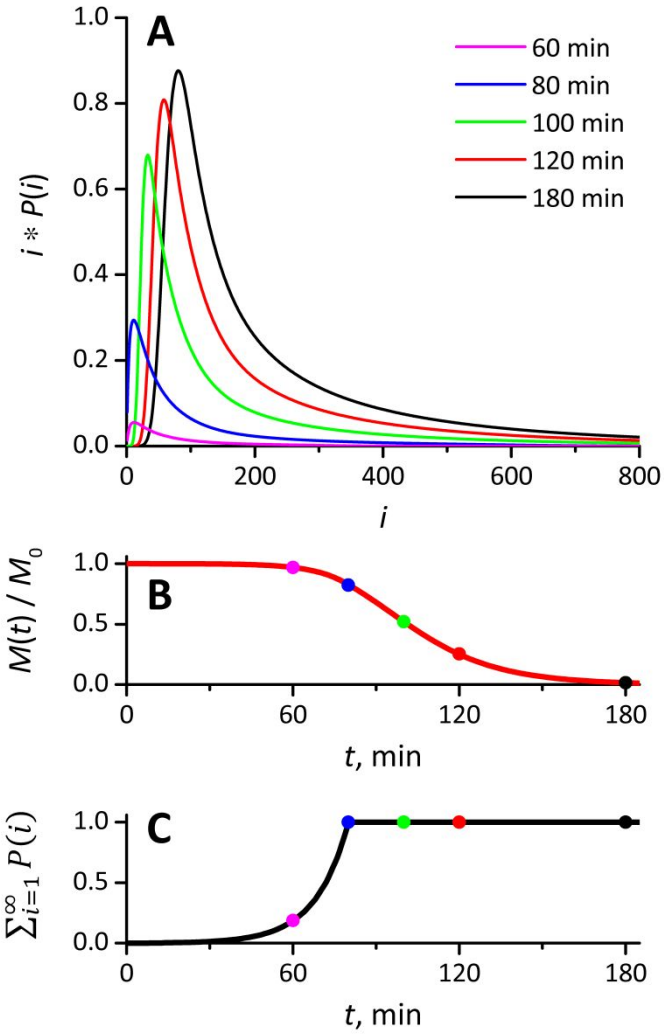

Figure 8. Detailed picture of the modeled polymerization process with exponentially increasing rate of initiator addition within 80 min. The chain propagation rate used for this Figure is that from Figure 2. (A) Snapshots of the distribution shown at different midway times indicated on the plot. (B) Fraction of the total amount of monomer left in the system as a function of time. (C) Fraction of the total number of polymer chains in the system as a function of time. The circles in panels (B) and (C) are color-coded to and indicate the times at which distributions in panel (A) were generated.

Another benefit of this model is the ability to simulate the MWDs for various new, yet unmeasured, initiator addition profiles. Figure S3 contains examples of the initiator addition rates, shown in the insets, which result in monomodal distributions. Figure S4, similarly to Figure S3, contains examples of the bimodal MWDs and their corresponding initiator addition profiles.

Furthermore, we improved the fits for the data sets Figure 3 and (A),(B) in Figure 4 where the model-experiment discrepancy was the largest for longer initiator addition times. Due to the fact that aggregation is a dynamic process which is dependent on the concentration of each chain size in solution, we determined customized $k_p(i)$ relationships for each type of addition profile and used them to better model the resultant MWDs. The improved distribution fits and the corresponding experimental data are shown in Figure 9. The modified chain propagation rates are available as insets. Notably, the fits for longer addition times are significantly improved using the optimized $k_p(i)$ vs i profile. The source of the deviations of the optimized rates from the effective rate in Figure 5 likely originates from the specific contribution of each chain length present in solution for different initiator addition profiles since different molar quantities of each chain length will result in distinct association equilibria. In this regard, it is interesting to point out that Figure 6 demonstrates that the customized effective $k_p(i)$ follow the same trend as the relationship found in the training data set. Also notable, increasing addition times, in general, induced a slight drop in $k_p(i)$, presumably due to a larger fraction of small polymer chains being present, which would shift the aggregation equilibrium marginally toward dormant species.

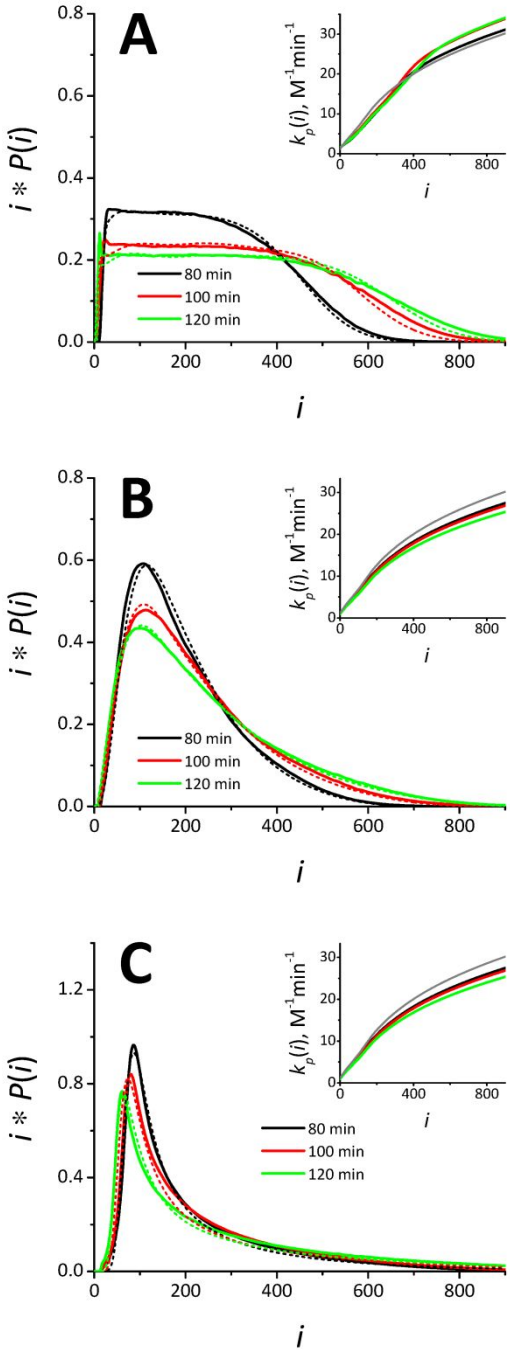

Figure 9. Experimental data (solid lines) and calculated curves (dashed lines) for the improved chain propagation rates, different for each curve in this Figure, see text for detail: (A) constant rate, (B) bell-shaped rate, and (C) exponentially increasing rate. Insets contain the chain propagation rates color-coded to the distributions generated from these rates. The solid grey lines in all insets are identical to Figure 2.

We then calculated dispersity ($Đ$), an important molecular weight distribution parameter, for various initiator addition times and compared these results to the values obtained directly from the size-exclusion chromatography data (Figure 10). The panels (A)-(D) of this Figure correspond to the initiator addition rates of the type shown in Figure 1(A)-(D). Solid blue lines with selected dots magnified in blue are obtained from the model, in a similar way to Figure 4, whereas the black dots correspond to the experimental data, and red dots are the improved fits from Figure 5 and 9. Interestingly, at shorter addition times the general model predicts dispersity values with high precision. However, the comparison between experimental and theoretical dispersity values shows a decreased accuracy of the general *effective* rate constant determined from the training set without any further modification (Figure 2). Modelling addition times of 80 min or higher results in larger deviations from experimental values. However, this can be substantially improved by using customized *effective* rate profiles. It is important to briefly note that the experimentally determined dispersity values may be slightly overestimated compared to the true dispersity values, though this effect is minimal.[48]

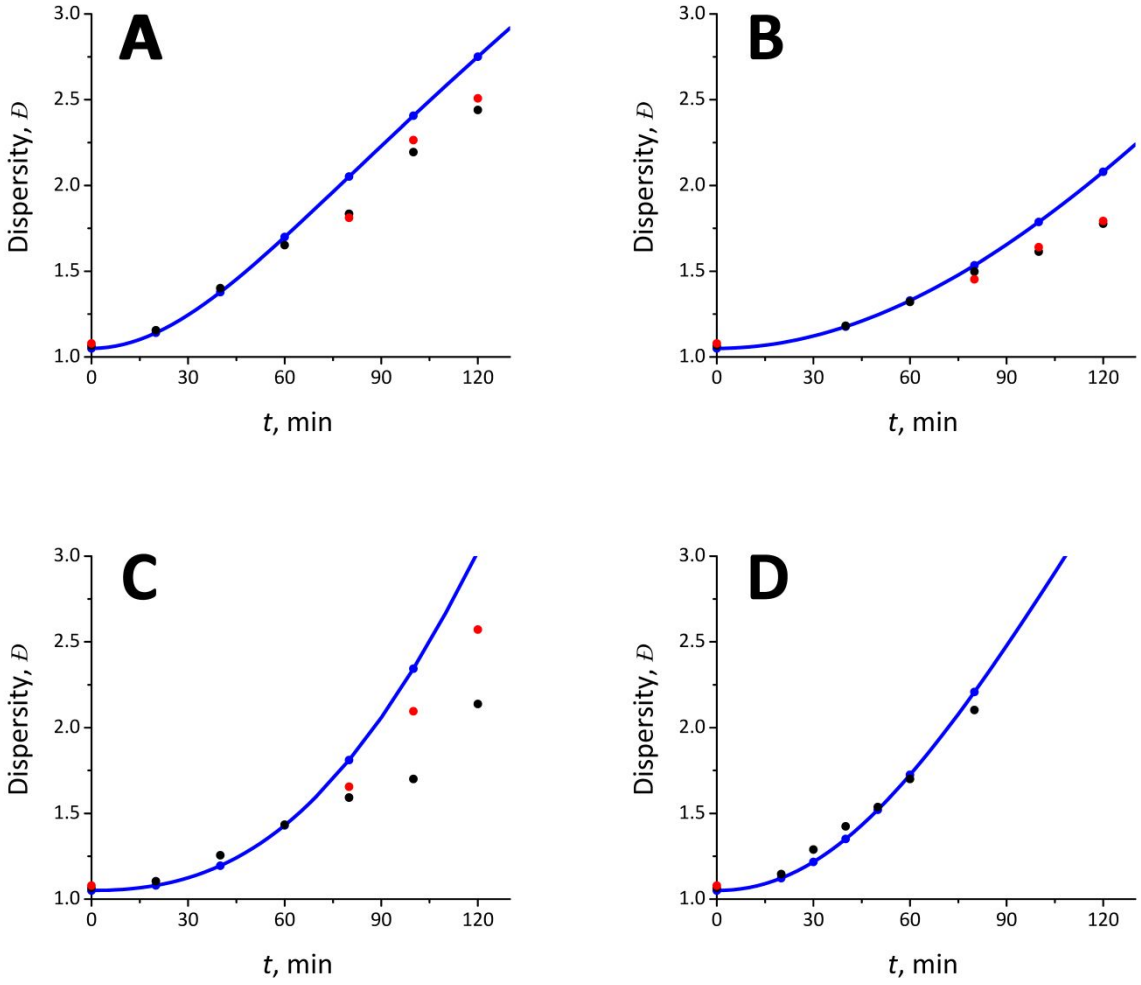

Figure 10. Dispersity (*Đ*), calculated for all the experiments discussed above: (A) constant rate, (B) bell-shaped rate, (C) exponentially increasing rate, and (D) linearly increasing rate. Solid blue lines (with selected cases magnified as blue circles) correspond to the effective rate constant, $k_p(i)$, given in Figure 2. Black circles represent dispersity calculated from the experimental data, whereas red circles are for the improved model fits as in Figure 9.

We then proceeded to examine the predictive behavior of our strategy by modeling MWDs prepared by more complex initiator addition profiles (shown in Figure 1E and F) which have not been previously reported, and in which the experimental MWDs were obtained after simulation. Similarly to the bell-shaped, exponentially increasing and linearly increasing initiator addition rates, without any modification, the effective propagation rate was found to satisfactory describe the more complex constant-then-exponentially-increasing rates of initiator addition demonstrated

in Figure 11A. The predicted (calculated) curves using the standard $k_p(i)$ vs i profile in Figure 2 retain the same shape as those achieved experimentally. The modeling of constant-then-exponentially-increasing rates accurately depicts the distribution shape but is less accurate in terms of overall fit. However, analogously to Figure 9, customized rates (Figure 11B) show improved fits and illustrate that even complex initiator addition rates can be predictably modeled with this theoretical strategy. Moreover, the calculated and experiment dispersity values (Figure 11C) were also improved with customized propagation rate constants. For the linearly decreasing initiator addition rates from Figure 1F the experimental MWDs were in good agreement with the precalculated MWDs, thus any improvement of the chain propagation rate for these two data sets was unnecessary. These sets of experiments demonstrate that MWDs can be predicted from a variety of previously unexplored initiator addition profiles and that the experimentally determined MWDs of the same rate profile match the predicted distribution functions with high fidelity.

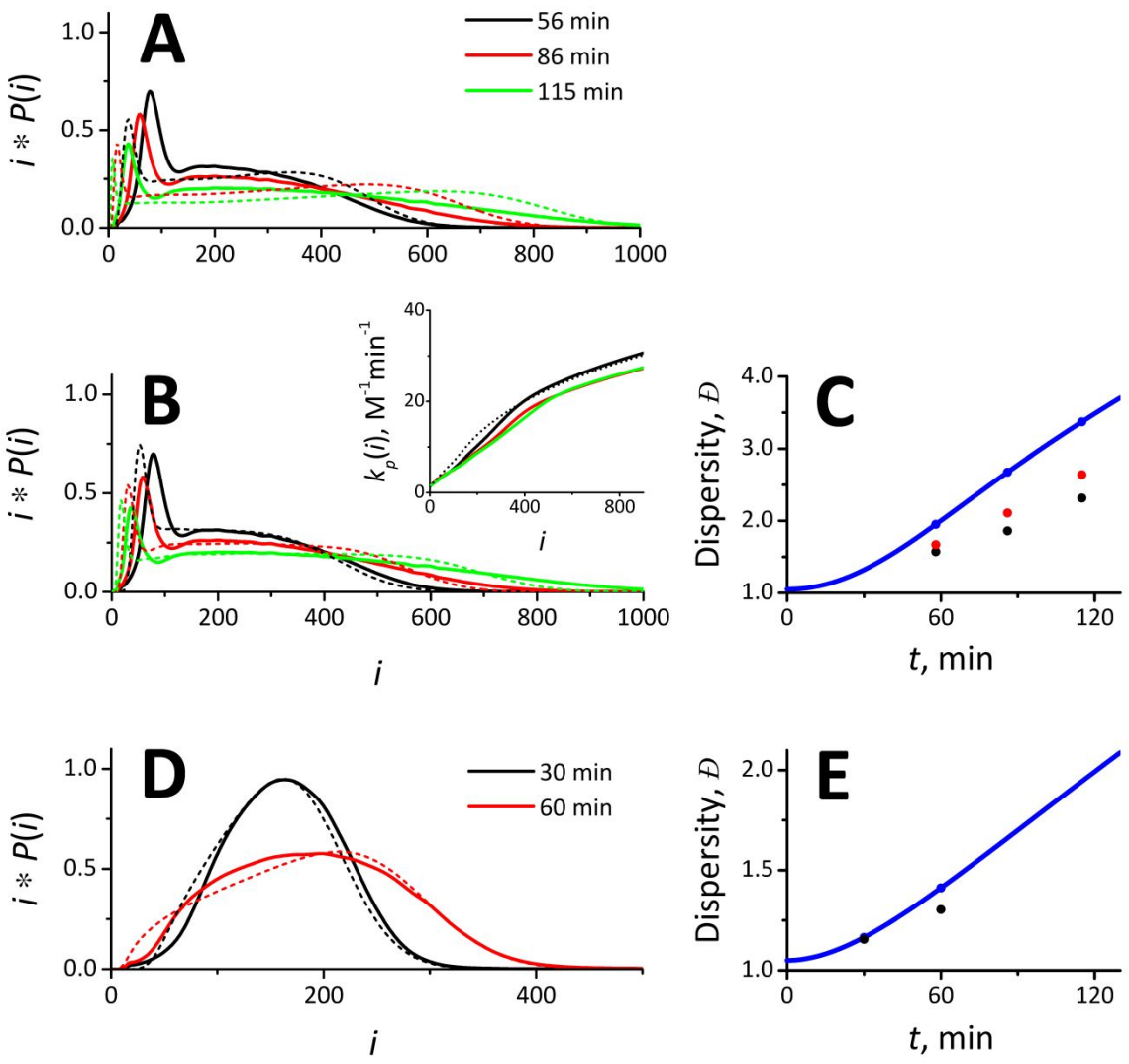

Figure 11. (A) Experimental data (solid lines) and model curves (dashed lines) calculated with the generic k_p from Figure 2 for the initiator addition rate in Figure 1E. (B) The same but for the improved rates illustrated in the inset. (C) Dispersity corresponding to the data in (A) and (B). Blue circles are for the model curves with generic k_p, red circles are for the model improved curves, and black circles were obtained from the experiment data. (D) Experimental data (solid lines) and model curves (dashed lines) calculated with the generic k_p from Figure 2 for the initiator addition rate in Figure 1F. (E) The same as (C) but for the data in (D).

Conclusions

Control of polymer MWD shape through temporal control of polymer chain initiation is rapidly becoming a robust handle for tuning material nanostructure and physical properties. This work has been driven by a desire to predict an arbitrary MWD and formulate an initiator addition profile that would produce it. In order to fully employ the shape of polymer MWDs as a versatile strategy to control polymer function, a predictive model is essential. We have outlined two modeling approaches that can be applied to this endeavor, and show how to utilize the second approach, with an effective chain propagation rate parameter, as well as how to fit the experimental data. We clearly demonstrate that this model reproduces experimental MWDs with high fidelity and provides novel physical insight into the dynamics of the polymerization process, such as simulating the MWDs for various new, yet unexplored, initiator addition profiles and calculating MWDs at times when monomer conversion is not complete. Interestingly, this model also describes the origin of increased rates of anionic polymerization for large polymer chains. We attribute this kinetic behavior to the complex relationship between propagation rate and the dynamics of heterogeneous mixtures of chain lengths, where longer chains have a lower affinity for association and thus propagate much faster. With the findings from this work, we anticipate that the use of polymer MWD shape to tailor material properties will proliferate, as initiation profiles for any arbitrary MWD can now be targeted through the use of this modeling approach.

Acknowledgments

This study was partially supported by Cornell University through the use of the Cornell Center for Materials Research shared facilities, which are supported by the NSF MRSEC program (DMR–1719875). B.P.F. thanks 3M for a Nontenured Faculty Award and the Sloan Research Foundation for a Sloan Research Fellowship.

References

(1) Lynd, N. A.; Meuler, A. J.; Hillmyer, M. A. Polydispersity and Block Copolymer Self-Assembly. *Prog. Polym. Sci.* **2008**, *33* (9), 875.

(2) Hustad, P. D.; Marchand, G. R.; Garcia-Meitin, E. I.; Roberts, P. L.; Weinhold, J. D. Photonic Polyethylene from Self-Assembled Mesophases of Polydisperse Olefin Block Copolymers. *Macromolecules* **2009**, *42* (11), 3788.

(3) Grubbs, R. B.; Grubbs, R. H. 50th Anniversary Perspective: Living Polymerization—Emphasizing the Molecule in Macromolecules. *Macromolecules* **2017**, *50* (18), 6979.

(4) Rubber Industry Sees Value in MWD. *Chem. Eng. News Arch.* **1965**, *43* (30), 40.

(5) Peplow, M. The Plastics Revolution: How Chemists Are Pushing Polymers to New Limits. *Nat. News* **2016**, *536* (7616), 266.

(6) Gentekos, D. T.; Dupuis, L. N.; Fors, B. P. Beyond Dispersity: Deterministic Control of Polymer Molecular Weight Distribution. *J. Am. Chem. Soc.* **2016**, *138* (6), 1848.

(7) Kottisch, V.; Gentekos, D. T.; Fors, B. P. "Shaping" the Future of Molecular Weight Distributions in Anionic Polymerization. *ACS Macro Lett.* **2016**, *5* (7), 796.

(8) Nadgorny, M.; Gentekos, D. T.; Xiao, Z.; Singleton, S. P.; Fors, B. P.; Connal, L. A. Manipulation of Molecular Weight Distribution Shape as a New Strategy to Control Processing Parameters. *Macromol. Rapid Commun.* **2017**, *38* (19), 1700352.

(9) Sides, S. W.; Fredrickson, G. H. Continuous Polydispersity in a Self-Consistent Field Theory for Diblock Copolymers. *J. Chem. Phys.* **2004**, *121* (10), 4974.

(10) Widin, J. M.; Schmitt, A. K.; Schmitt, A. L.; Im, K.; Mahanthappa, M. K. Unexpected Consequences of Block Polydispersity on the Self-Assembly of ABA Triblock Copolymers. *J. Am. Chem. Soc.* **2012**, *134* (8), 3834.

(11) Lynd, N. A.; Hillmyer, M. A. Influence of Polydispersity on the Self-Assembly of Diblock Copolymers. *Macromolecules* **2005**, *38* (21), 8803.

(12) Li, S.; Register, R. A.; Weinhold, J. D.; Landes, B. G. Melt and Solid-State Structures of Polydisperse Polyolefin Multiblock Copolymers. *Macromolecules* **2012**, *45* (14), 5773.

(13) Cooke, D. M.; Shi, A.-C. Effects of Polydispersity on Phase Behavior of Diblock Copolymers. *Macromolecules* **2006**, *39* (19), 6661.

(14) Oschmann, B.; Lawrence, J.; Schulze, M. W.; Ren, J. M.; Anastasaki, A.; Luo, Y.; Nothling, M. D.; Pester, C. W.; Delaney, K. T.; Connal, L. A. Effects of Tailored

Dispersity on the Self-Assembly of Dimethylsiloxane–Methyl Methacrylate Block Co-Oligomers. *ACS Macro Lett.* **2017**, *6* (7), 668.

(15) Nichetti, D.; Manas-Zloczower, I. Influence of Molecular Parameters on Material Processability in Extrusion Processes. *Polym. Eng. Sci.* **1999**, *39* (5), 887.

(16) Listak, J.; Jakubowski, W.; Mueller, L.; Plichta, A.; Matyjaszewski, K.; Bockstaller, M. R. Effect of Symmetry of Molecular Weight Distribution in Block Copolymers on Formation of "Metastable" Morphologies. *Macromolecules* **2008**, *41* (15), 5919.

(17) Meira, G. R.; Johnson, A. F. Molecular Weight Distribution Control in Continuous "Living" Polymerizations through Periodic Operation of the Monomer Feed. *Polym. Eng. Sci.* **1981**, *21* (7), 415.

(18) Alassia, L. M.; Couso, D. A.; Meira, G. R. Molecular Weight Distribution Control in a Semibatch Living-Anionic Polymerization. II. Experimental Study. *J. Appl. Polym. Sci.* **1988**, *36* (3), 481.

(19) Couso, D. A.; Alassia, L. M.; Meira, G. R. Molecular Weight Distribution Control in a Semibatch "Living" Anionic Polymerization. I. Theoretical Study. *J. Appl. Polym. Sci.* **1985**, *30* (8), 3249.

(20) Laurence, R. L.; Vasudevan, G. Performance of a Polymerization Reactor in Periodic Operation. *Ind. Eng. Chem. Process Des. Dev.* **1968**, *7* (3), 427.

(21) Hungenberg, K.-D.; Knoll, K.; Wulkow, M. Absolute Propagation Rate Coefficients in Radical Polymerization from Gel Permeation Chromatography of Polymers Produced by Intermittent Initiation. *Macromol. Theory Simul.* **1997**, *6* (2), 393.

(22) Farkas, E.; Meszena, Z. G.; Johnson, A. F. Molecular Weight Distribution Design with Living Polymerization Reactions. *Ind. Eng. Chem. Res.* **2004**, *43* (23), 7356.

(23) Gosden, R. G.; Meszena, Z. G.; Mohsin, M. A.; Auguste, S.; Johnson, A. F. Living Polymerisation Reactors. Part II. Theoretical and Experimental Tests on an Algorithm Which Predicts Mwds From CSTRs with Perturbed Feeds. *Polym. React. Eng.* **1997**, *5* (1–2), 45.

(24) Seno, K.-I.; Kanaoka, S.; Aoshima, S. Thermosensitive Diblock Copolymers with Designed Molecular Weight Distribution: Synthesis by Continuous Living Cationic Polymerization and Micellization Behavior. *J. Polym. Sci. Part Polym. Chem.* **2008**, *46* (6), 2212.

(25) Gentekos, D. T.; Jia, J.; Tirado, E. S.; Barteau, K. P.; Smilgies, D.-M.; DiStasio, R. A.; Fors, B. P. Exploiting Molecular Weight Distribution Shape to Tune Domain Spacing in Block Copolymer Thin Films. *J. Am. Chem. Soc.* **2018**, *140* (13), 4639.

(26) Li, H.; Collins, C. R.; Ribelli, T. G.; Matyjaszewski, K.; Gordon, G. J.; Kowalewski, T.; Yaron, D. J. Tuning the Molecular Weight Distribution from Atom Transfer Radical Polymerization Using Deep Reinforcement Learning. *Mol. Syst. Des. Eng.*, **2018**, 3, 496.

(27) Corrigan, N.; Manahan, R.; Lew, Z. T.; Yeow, J.; Xu, J.; Boyer, C. Copolymers with Controlled Molecular Weight Distributions and Compositional Gradients through Flow Polymerization. *Macromolecules*, **2018**, 51 (12), 4553.

(28) Corrigan, N.; Almasri, A.; Taillades, W.; Xu, J.; Boyer, C. Controlling Molecular Weight Distributions through Photoinduced Flow Polymerization. *Macromolecules*, **2017**, 50 (21), 8438.

(29) Sanchez, I. C. Irreversible Anionic Polymerization Kinetics Revisited. *Ind. Eng. Chem. Res.* **2010**, *49* (23), 11890.

(30) Frontini, G. L.; Eliçabe, G. E.; Couso, D. A.; Meira, G. R. Optimal Periodic Control of a Continuous "Living" Anionic Polymerization. I. Theoretical Study. *J. Appl. Polym. Sci.* **1986**, *31* (4), 1019.

(31) Frontini, G. L.; Eliçabe, G. E.; Meira, G. R. Optimal Periodic Control of a Continuous "Living" Anionic Polymerization II. New Theoretical Results. *J. Appl. Polym. Sci.* **1987**, *33* (6), 2165.

(32) Costa, M. R. P. F. N.; Dias, R. C. S. An Improved General Kinetic Analysis of Non-Linear Irreversible Polymerisations. *Chem. Eng. Sci.* **2005**, *60* (2), 423.

(33) Quinebèche, S.; Navarro, C.; Gnanou, Y.; Fontanille, M. In Situ Mid-IR and UV–visible Spectroscopies Applied to the Determination of Kinetic Parameters in the Anionic Copolymerization of Styrene and Isoprene. *Polymer* **2009**, *50* (6), 1351.

(34) Tsvetanov, K.; Mueller, A. H. E.; Schulz, G. V. Dependence of the Propagation Rate Constants on the Degree of Polymerization in the Initial Stage of the Anionic Polymerization of Methyl Methacrylate in Tetrahydrofuran. *Macromolecules* **1985**, *18* (5), 863.

(35) Morton, M.; Fetters, L. J.; Pett, R. A.; Meier, J. F. The Association Behavior of Polystyryllithium, Polyisoprenyllithium, and Polybutadienyllithium in Hydrocarbon Solvents. *Macromolecules* **1970**, 3, 327.

(36) Worsford, D. J.; Bywater, S. Degree of Association of Polystyryl-, Polyisoprenyl-, and Polybutadienyllithium in Hydrocarbon Solvents. *Macromolecules* **1972**, 5, 393.

(37) Wittig, V. G.; Meyer, F. J.; Lange, G. On the Behavior of Diphenyl Metals as Complexing Agents. *Ann.* **1951**, 571, 167.

(38) Morita, H.; Van Beylen, M. New Vistas on the Anionic Polymerization of Styrene in Non-Polar Solvents by Means of Density Functional Theory. *Polymers* **2016**, *8* (10), 371.

(39) Buback, M.; Egorov, M.; Gilbert, R. G.; Kaminsky, V.; Olaj, O. F.; Russell, G. T.; Vana, P.; Zifferer, G. Critically Evaluated Termination Rate Coefficients for Free-Radical Polymerization, 1 The Current Situation. *Macromol. Chem. Phys.* **2002**, *203* (18), 2570.

(40) Buback, M.; Garcia-Rubio, L. H.; Napper, D. H.; Guillot, J.; Hamielec, A. E.; Hill, D.; O'Driscoll, K. F.; Olaj, O. F.; Shen, J.; Solomon, D.; Moad, G.; Stickler, M.; Tirrell, M.; Winnik, M. A. Consistent Values of Rate Parameters in Free Radical Polymerization Systems. *J. Polym. Sci., Part C: Phys. Lett.* **1998**, 26, 293.

(41) Buback, M.; Busch, M.; Kowollik, C. Chain-length Dependence of Free-Radical Termination Rate Deduced from Laser Single-Pulse Experiments. *Macromol. Theory Simul.* **2000**, *9* (8), 442.

(42) Worsfold, D. J.; Bywater, S. Anionic Polymerization of Styrene. *Can. J. Chem.* **1960**, *38* (10), 1891.

(43) Bywater, S.; Worsfold, D. J. Alkyllithium Anionic Polymerization Initiators in Hydrocarbon Solvents. *J. Organomet. Chem.* **1967**, *10* (1), 1.

(44) Lühmann, N.; Niu, A.; Allgaier, J.; Stellbrink, J.; Zorn, R.; Linnolahti, M.; Willbold, S.; Koenig, B. W.; Grillo, I.; Richter, D.; et al. The Initiation Mechanism of Butadiene Polymerization in Aliphatic Hydrocarbons: A Full Mechanistic Approach. *Macromolecules* **2016**, *49* (15), 5397.

(45) Alger, Mark. Polymer Science Dictionary. New York: Elsevier Applied Science, 1989, 28.

(46) Fehlberg, E. Classical Fourth- and Lower Order Runge-Kutta Formulas with Stepsize Control and Their Application to Heat Transfer Problems. Computing 1970, *6* (1), 61.

(47) Shampine, L. F.; Watts, H. A.; Davenport, S. M. Solving Nonstiff Ordinary Differential Equations - The State of the Art. *SIAM Rev.* **1976**, *18*, 376.

(48) Lee, W.: Lee, H.; Cha, J.; Chang, T.; Hanley, K. J.; Lodge, T. P. Molecular Weight Distribution of Polystyrene Made by Anionic Polymerization **2000**, *33* (14), 376.

Table of Contents Graphic